The effects of LIGO detector noise on a 15-dimensional Markov-chain Monte Carlo analysis of gravitational-wave signals

V Raymond[1]**, M V van der Sluys**[2]**, I Mandel**[1]**, V Kalogera**[1]**, C Röver**[3] **and N Christensen**[4]

[1] Department of Physics & Astronomy, Northwestern University, 2131 Tech Drive, Evanston, IL 60 208, USA
[2] Department of Physics, University of Alberta, 11322-89 Avenue, Edmonton AB, T6G 2G7, Canada
[3] Max-Planck-Institut für Gravitationsphysik, Callinstraße 38, 30167 Hannover, Germany
[4] Physics & Astronomy Department, Carleton College, One North College Street, Northfield, MN 55057, USA

E-mail: vivien@u.northwestern.edu

Abstract

Gravitational-wave signals from inspirals of binary compact objects (black holes and neutron stars) are primary targets of the ongoing searches by ground-based gravitational-wave (GW) interferometers (LIGO, Virgo and GEO-600). We present parameter estimation results from our Markov-chain Monte Carlo code SPINSPIRAL on signals from binaries with precessing spins. Two data sets are created by injecting simulated GW signals either into synthetic Gaussian noise or into LIGO detector data. We compute the 15-dimensional probability-density functions (PDFs) for both data sets, as well as for a data set containing LIGO data with a known, loud artefact ('glitch'). We show that the analysis of the signal in detector noise yields accuracies similar to those obtained using simulated Gaussian noise. We also find that while the Markov chains from the glitch do not converge, the PDFs would look consistent with a GW signal present in the data. While our parameter estimation results are encouraging, further investigations into how to differentiate an actual GW signal from noise are necessary.

PACS numbers: 02.50.−r, 02.70.Uu, 04.30.Tv, 04.80.Nn, 95.85.Sz

(Some figures in this article are in colour only in the electronic version)

1. Introduction

Among the sources of gravitational waves (GWs), inspiralling binary systems of compact objects, neutron stars (NSs) and/or black holes (BHs) in the mass range $\sim 1\, M_\odot$–$100\, M_\odot$ stand out as likely to be detected and relatively easy to model. For ground-based laser interferometers currently in operation (Cutler and Thorne 2002), LIGO (Abbott *et al* 2009a), Virgo (Acernese *et al* 2008) and GEO-600 (Willke *et al* 2004), the current detection-rate estimates for BH-NS binaries range from 2×10^{-4} to $0.2\ \mathrm{yr}^{-1}$ for first-generation instruments (e.g. O'Shaughnessy *et al* 2008, Abadie *et al* 2010). Although the estimates are quite uncertain, detection rates are expected to increase with the upgrade to Enhanced LIGO/Virgo, up to $\sim 40\ \mathrm{yr}^{-1}$ with Advanced LIGO/Virgo.

The detection of a gravitational-wave event is challenging and will be a rewarding achievement by itself. After such a detection, measurement of source properties holds major promise for improving our astrophysical understanding and requires reliable methods for parameter estimation. This is a complicated problem because of the large number of parameters (15 for spinning compact objects in a quasi-circular orbit) and the degeneracies between them (Raymond *et al* 2009), the significant amount of structure in the parameter space and the particularities of the detector noise.

In this paper we use an example to illustrate the capabilities of our Markov-chain Monte Carlo (MCMC) algorithm SPINSPIRAL (Van der Sluys *et al* 2008a) for parameter estimation of binary inspirals with two spinning components, using ground-based GW interferometers. In these proceedings we focus on the effects of using LIGO detector data versus synthetic Gaussian noise. Earlier studies (e.g. Jaranowski and Krolak 1994, Cutler and Flanagan 1994, Poisson and Will 1995, Van den Broeck and Sengupta 2007) computed the potential accuracy of parameter estimation (e.g. by using the Fisher matrix), but without performing a parameter estimation in practice. Also, Röver *et al* (2006), (2007), (2006), (2008a) explored parameter estimation for binaries without spins, described by nine parameters.

We present the gravitational-wave template used for this study in section 2, and the Bayesian framework we employ here in section 3. In section 4.1 we describe the three data sets that we analyse in this study: a simulated GW signal injected into synthetic Gaussian noise, a GW signal injected into LIGO detector data and a raw LIGO data set containing a known artefact of terrestrial origin ('glitch'). We describe the details of the MCMC simulations in section 4.2. The analyses of the first two data sets are compared in section 4.3, and we present our results on the glitch in section 4.4.

2. Gravitational-wave signal and observables

We analyse the signal produced during the inspiral phase of two compact objects of masses $M_{1,2}$ in quasi-circular orbit. We focus on a black hole binary system with $M_1 = 10\, M_\odot$ and $M_2 = 1.4\, M_\odot$, where unlike in some of our previous studies (e.g. Van der Sluys *et al* 2008b), we do not ignore the second spin to explore the single-spin approximation. During the orbital inspiral, the general-relativistic spin–orbit and spin–spin couplings (dragging of inertial frames) cause the binary's orbital plane to precess and introduce amplitude and phase modulations of the observed gravitational-wave signal (Apostolatos *et al* 1994).

A circular binary inspiral with both compact objects spinning is described by a 15-dimensional parameter vector $\vec{\lambda} \in \Lambda$. Our choice of independent parameters with respect to a fixed geocentric coordinate system is

$$\vec{\lambda} = \{\mathcal{M}, \eta, \log d_{\mathrm{L}}, t_{\mathrm{c}}, \phi_{\mathrm{c}}, \alpha, \cos\delta, \sin\iota, \psi,$$

$$a_{\mathrm{spin1}}, \cos\theta_{\mathrm{spin1}}, \phi_{\mathrm{spin1}}, a_{\mathrm{spin2}}, \cos\theta_{\mathrm{spin2}}, \phi_{\mathrm{spin2}}\}, \tag{1}$$

where $\mathcal{M} = \frac{(M_1 M_2)^{3/5}}{(M_1+M_2)^{1/5}}$ and $\eta = \frac{M_1 M_2}{(M_1+M_2)^2}$ are the chirp mass and symmetric mass ratio, respectively; d_{L} is the luminosity distance to the source; ϕ_{c} is an integration constant that specifies the GW phase at the time of coalescence t_{c}, defined with respect to the centre of the Earth; α (right ascension) and δ (declination) identify the source position in the sky; ι defines the inclination of the binary with respect to the line of sight; and ψ is the polarization angle of the waveform. The spins are specified by $0 \leqslant a_{\mathrm{spin}_{1,2}} \equiv S_{1,2}\big/M_{1,2}^2 \leqslant 1$ as the dimensionless spin magnitude, and the angles $\theta_{\mathrm{spin}1,2}, \phi_{\mathrm{spin}1,2}$ for their orientations.

Given a network comprising n_{det} detectors, the data collected at the *a*th instrument ($a = 1, \ldots, n_{\mathrm{det}}$) are given by $x_a(t) = n_a(t) + h_a(t; \vec{\lambda})$, where $h_a(t; \vec{\lambda}) = F_{a,+}(t, \alpha, \delta, \psi)\, h_{a,+}(t; \vec{\lambda}) + F_{a,\times}(t, \alpha, \delta, \psi)\, h_{a,\times}(t; \vec{\lambda})$ is the GW strain at the detector (see equations (2)–(5) in Apostolatos *et al* (1994)) and $n_a(t)$ is the detector noise. The astrophysical signal is given by the linear combination of the two independent polarizations $h_{a,+}(t; \vec{\lambda})$ and $h_{a,\times}(t; \vec{\lambda})$ weighted by the antenna beam patterns $F_{a,+}(t, \alpha, \delta, \psi)$ and $F_{a,\times}(t, \alpha, \delta, \psi)$.

The waveform we use includes terms up to 3.5-post-Newtonian (pN) order in phase and uses Newtonian amplitudes, with spin effects up to 2.5 pN in phase. We generate the waveform templates using the routine `LALGenerateInspiral()` with the approximant `SpinTaylor` from the injection package in the LSC Algorithm Library (LAL) (LIGO Scientific Collaboration 2007), which closely follows the first section of Buonanno *et al* (2003).

3. Parameter estimation: methods

In our Bayesian analysis we use MCMC methods to determine the multi-dimensional *posterior* probability-density function (PDF) of the unknown parameter vector $\vec{\lambda}$ in equation (1), given the data sets x_a collected by a network of n_{det} detectors, a model M of the waveform and the *prior* $p(\vec{\lambda})$ on the parameters. Our priors are uniform in the parameters of equation (1) (see Van der Sluys *et al* (2008a) for details). One can compute the probability density via Bayes' theorem

$$p(\vec{\lambda}|x_a, M) = \frac{p(\vec{\lambda}|M)\, p(x_a|\vec{\lambda}, M)}{p(x_a|M)}, \tag{2}$$

where

$$\mathcal{L} \equiv p(x_a|\vec{\lambda}, M) \propto \exp\left(\langle x_a|h_a(\vec{\lambda})\rangle - \tfrac{1}{2}\langle h_a(\vec{\lambda})|h_a(\vec{\lambda})\rangle\right) \tag{3}$$

is the *likelihood function*, which measures how well the data fit the model M for the parameter vector $\vec{\lambda}$. The term $p(x_a|M)$ is the *marginal likelihood* or *evidence*. In the previous equation

$$\langle x|y\rangle = 4\mathrm{Re}\left(\int_{f_{\mathrm{low}}}^{f_{\mathrm{high}}} \frac{\tilde{x}(f)\tilde{y}^*(f)}{S_a(f)}\, \mathrm{d}f\right) \tag{4}$$

is the *overlap* of signals x and y, $\tilde{x}(f)$ is the Fourier transform of $x(t)$ and $S_a(f)$ is the noise power-spectral density in the detector a. The likelihood computed for the injection parameters $\mathcal{L}_{\mathrm{inj}} = p(x_a|\vec{\lambda}_{\mathrm{inj}}, M)$ is then a random variable that depends on the particular noise realization n_a in the data $x_a = h(\vec{\lambda}_{\mathrm{inj}}) + n_a$. The injection parameters are the parameters of the waveform template added to the noise. We define the signal-to-noise ratio (SNR) of the injection to be

$$\mathrm{SNR} = \frac{\langle x|h(\vec{\lambda}_{\mathrm{inj}})\rangle}{\sqrt{\langle h(\vec{\lambda}_{\mathrm{inj}})|h(\vec{\lambda}_{\mathrm{inj}})\rangle}}. \tag{5}$$

From here on, we use the expected value of the SNR, which is equal to the square root of twice the expectation value of $\log \mathcal{L}_{\text{inj}}$:

$$\text{SNR} = \sqrt{\langle h(\vec{\lambda}_{\text{inj}}) | h(\vec{\lambda}_{\text{inj}}) \rangle}. \tag{6}$$

To combine observations from a network of detectors with uncorrelated noise realizations (this is the case in this paper as we use two non-co-located detectors), we have the likelihood $p(\vec{x}|\vec{\lambda}, M) = \prod_{a=1}^{n_{\text{det}}} p(x_a|\vec{\lambda}, M)$, for $\vec{x} \equiv \{x_a : a = 1, \ldots, n_{\text{det}}\}$, and

$$p(\vec{\lambda}|\vec{x}, M) = \frac{p(\vec{\lambda}|M) \, p(\vec{x}|\vec{\lambda}, M)}{p(\vec{x}|M)}. \tag{7}$$

The numerical computation of the PDF involves the evaluation of a large multi-modal, multi-dimensional integral. Markov-chain Monte Carlo (MCMC) methods (e.g. Gilks *et al* 1996, Gelman *et al* 1997, and references therein) have proved to be especially effective in tackling this numerical problem. We developed an adaptive (see Figueiredo and Jain 2002, Atchadé and Rosenthal 2005) MCMC algorithm to explore the parameter space Λ efficiently while requiring the least amount of tuning for the specific signal analysed; the code is an extension of the one developed by some of the authors to explore MCMC methods for binaries without spin (Röver *et al* 2006, 2007). We implemented parallel tempering (Hukushima and Nemoto 1996, Hansmann 1997, Röver 2007) to improve the sampling. It consists of running several MCMC chains in parallel, each with a different 'temperature', which can swap parameters under certain conditions. Only the $T = 1$ chain is currently used for post-processing.

In equation (7) we applied Bayes' theorem to obtain the probability of a specific parameter vector value ($\vec{\lambda}$) given the observed data $\vec{x}$ and the model M. The theorem can also be applied to compute the probability of a specific *model M_i* given the observed data:

$$p(M_i|\vec{x}) = \frac{p(M_i) \, p(\vec{x}|M_i)}{p(\vec{x})}. \tag{8}$$

We compare the two models M_i and M_j by computing the *odds ratio*

$$O_{i,j} = \frac{p(M_i|\vec{x})}{p(M_j|\vec{x})} = \frac{p(M_i) \, p(\vec{x}|M_i)}{p(M_j) \, p(\vec{x}|M_j)} = \frac{p(M_i)}{p(M_j)} B_{i,j}, \tag{9}$$

where

$$B_{i,j} = \frac{p(\vec{x}|M_i)}{p(\vec{x}|M_j)} \tag{10}$$

is the *Bayes factor* of the two models, and we recognize the evidence $p(\vec{x}|M_i)$ from equation (7). The evidence must be marginalized over the parameters of the model in order to compute the Bayes factor:

$$p(\vec{x}|M_i) = \int_{\Lambda} p(\vec{\lambda}|M_i) \, p(\vec{x}|\vec{\lambda}, M_i) \, \text{d}\vec{\lambda}. \tag{11}$$

There are existing algorithms dedicated to the computation of this integral, and of the Bayes factor. For instance, *nested sampling* (Skilling 2006) has been shown to be very efficient in the case of non-spinning gravitational-wave sources (Veitch and Vecchio 2009), and can in addition be used to produce PDFs of the parameters. As a by-product of the exploration of the parameter space with MCMC, it is possible to compute the evidence of the models used. We have implemented the harmonic-mean method (Newton and Raftery 1994), in which the evidence is approximated by

$$p(\vec{x}|M_i) \approx \sum_{k=1}^{N} p(\vec{\lambda}_k|M_i) \, p(\vec{x}|\vec{\lambda}_k, M_i) V_{\vec{\lambda}_k}, \tag{12}$$

where $\{\vec{\lambda}_k : k = 1, \ldots, N\}$ is the set of N points sampled by the MCMC, and $V_{\vec{\lambda}_k}$ is the volume of parameter space associated with the point $\vec{\lambda}_k$. Since the MCMC algorithm samples according to the posterior (and, up to a proportionality constant, converges towards posterior PDF), the density of points in the chain at a certain location $\vec{\lambda}_k$ in the parameter space Λ will become proportional to the posterior for large N. It follows that

$$\lim_{N \to \infty} V_{\vec{\lambda}_k} = \frac{\alpha_i}{p(\vec{\lambda}_k | M_i) \, p(\vec{x} | \vec{\lambda}_k, M_i)}, \tag{13}$$

where α_i a proportionality constant. We then have $p(\vec{x} | M_i) \approx \sum_{k=1}^{N} \alpha_i = N \alpha_i$, and obtain the estimate for α_i by considering the whole parameter space volume V_t:

$$V_t \approx \sum_{k=1}^{N} V_{\vec{\lambda}_k} = \sum_{k=1}^{N} \frac{\alpha_i}{p(\vec{\lambda}_k | M_i) \, p(\vec{x} | \vec{\lambda}_k, M_i)}. \tag{14}$$

Finally,

$$p(\vec{x} | M_i) \approx N V_t \left[\sum_{k=1}^{N} \frac{1}{p(\vec{\lambda}_k | M_i) \, p(\vec{x} | \vec{\lambda}_k, M_i)} \right]^{-1}, \tag{15}$$

which is the harmonic mean of the posterior values sampled by the MCMC. The issue with this method is that it gives too much weight to low-posterior points, which lie in a part of the parameter space that is badly sampled, by design, by the MCMC. The estimate of the evidence is then very sensitive to the quality of the sampling of a particular run. We are looking into other algorithms in order to remedy this problem, e.g. by using the higher temperature chains produced by parallel tempering (Earl and Deem 2005) (we currently use the $T = 1$ chain only), or by using a well-sampled subset of points (Van Haasteren 2009) to estimate the probability constant α_i. A summary of the methods used in our MCMC code was published in Van der Sluys *et al* (2008a): a more complete technical description of the SPINSPIRAL code will be available in Van der Sluys *et al* (in preparation).

4. Parameter estimation: results

4.1. Data sets

For these proceedings, we analyse three different data sets, each containing the data for the 4 km LIGO detectors at Hanford (H1) and Livingston (L1):

DS1: a coherent software injection with a total SNR of 11.3 into synthetic Gaussian, stationary noise, simulated for the H1 and L1 detectors;

DS2: a coherent software injection of the same signal, with a total SNR of 11.3, into 'quiet' LIGO detector data from H1 and L1;

DS3: raw LIGO data from H1 and L1, containing a known, coincident glitch of seismic origin, with a total SNR of 11.3.

For the data sets DS1 and DS2, the injected signal is that of a 10 $M_{\odot}$ spinning BH and a 1.4 $M_{\odot}$ spinning NS in an inspiralling binary system. A low-mass Compact Binary Coalescence Group search (Abbott *et al* 2009b) does not produce a GW trigger for the data segment DS2; hence we designate it 'quiet'. The distance of each of the injections is scaled to obtain an SNR of 11.3, equal to that of the glitch in DS3, but computed with different waveforms: a SpinTaylor waveform (see section 2) for DS1 and DS2, and a non-spinning, 2-pN waveform (see

section 4.4) for DS3. The other parameters of the injection are

$$\vec{\lambda} = \{\mathcal{M} = 2.99\,M_{\odot}, \eta = 0.107, d_{\mathrm{L}}, t_{\mathrm{c}}, \phi_{\mathrm{c}} = 85.9^{\circ}, \alpha = 17.4\,h, \delta = 61.6^{\circ},$$
$$i = 52.8^{\circ}, \psi = 11.6^{\circ}, a_{\mathrm{spin1}} = 0.6, \theta_{\mathrm{spin1}} = 78.5^{\circ}, \phi_{\mathrm{spin1}} = 63.0^{\circ},$$
$$a_{\mathrm{spin2}} = 0.4, \theta_{\mathrm{spin2}} = 120.0^{\circ}, \phi_{\mathrm{spin2}} = 315.1^{\circ}\}, \tag{16}$$

where we assigned a spin of 0.4 to the neutron star, which is higher than astrophysically plausible, for testing purposes only. In DS3, no signal is injected. For our analyses, we use the data of both 4 km LIGO detectors H1 and L1.

4.2. MCMC simulations

The MCMC analysis that we carry out on each data set consists of ten independent Markov chains, each with a length of about a million iterations and composed of five chains at different temperatures for parallel tempering. From now on, we will refer to the $T = 1$ chain as *the chain*, since the hotter chains were not used in the post-processing. The part of the chains that is analysed is that after the *burn-in* period (see e.g. Gilks *et al* (1996)), the length of which is determined automatically as follows: we determine the absolute maximum likelihood $\log(\mathcal{L}_{\mathrm{max}})$, defined as the highest value for $\log[p(\vec{x}|\vec{\lambda}, M)]$ obtained over the ensemble of parameter sets $\vec{\lambda}$ in any of our individual Markov chains. Then for each chain we include all the iterations *after* the chain reaches a likelihood value of $\log(\mathcal{L}_{\mathrm{max}}) - 2$ for the first time. This results in a convergence test as well, since some of the independent chains may not reach this threshold value. Typically, we demand that more than 50% of our chains meet this condition before we consider the MCMC run as *converged*, although we consider results as *robust* if they have a convergence rate of 80% or more. This convergence test is a measure of the quality of our sampling in a given number of iterations. All our Markov chains start at values that are randomly offset from the injection values. The starting values for $\mathcal{M}$ and t_{c} are drawn from a Gaussian distribution centred on the injection value, with a standard deviation of $0.025\,M_{\odot}$ and 10 ms respectively. In real analysis, the two Gaussian distributions are centred on the values from the template bank-based search of the Compact Binary Coalescence group (Abbott *et al* 2009b) which will have triggered the MCMC followup. The other 13 parameters are drawn uniformly from their allowed ranges. SPINSPIRAL needs to run for typically a few days in order to show the first results and a week or two to accumulate a sufficient number of iterations for good statistics, each chain using a single 2.8 GHz CPU.

4.3. Analysis of data sets DS1 and DS2

We analysed the data sets DS1 and DS2 as described in section 4.1 and the results of both analyses passed the convergence test described in section 4.2 with convergence rates of 70% and 80%, respectively. The resulting one-dimensional marginalized PDFs from both analyses are shown in figure 1.

Table 1 shows the median and the width of the 95%-probability ranges for each parameter. The differences we find between the results for DS1 and DS2 may be attributed to the particular noise realizations in this example, and most parameters yield similar PDFs and accuracies.

The PDFs of the parameters that describe the spin of the NS follow the prior distributions in both runs. This justifies ignoring the NS spin (by fixing a_{spin2} to 0.0 in the recovery template) for this mass ratio (Van der Sluys *et al* 2008b). For each of the two data sets, DS1 and DS2, we computed the Bayes factor to compare the evidence for the following two models: M_1: a 3.5-pN inspiral waveform embedded in Gaussian noise and M_2: Gaussian noise only. The values are listed in table 2. In both cases, the Bayes factor is large, providing strong evidence
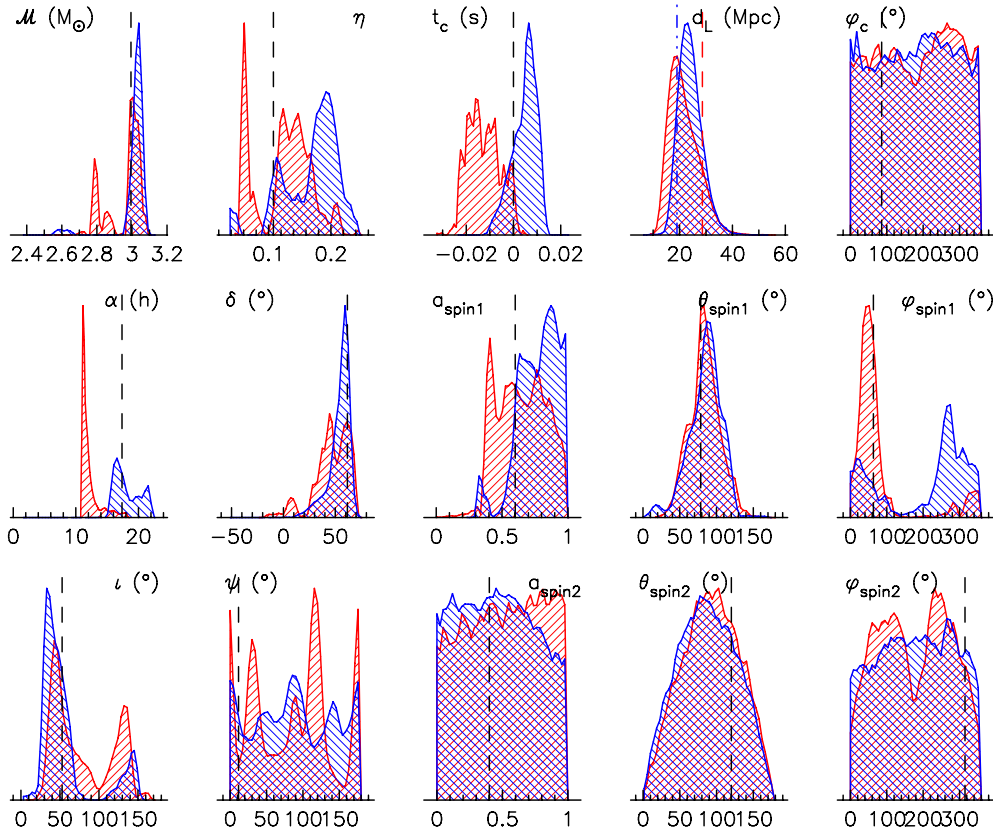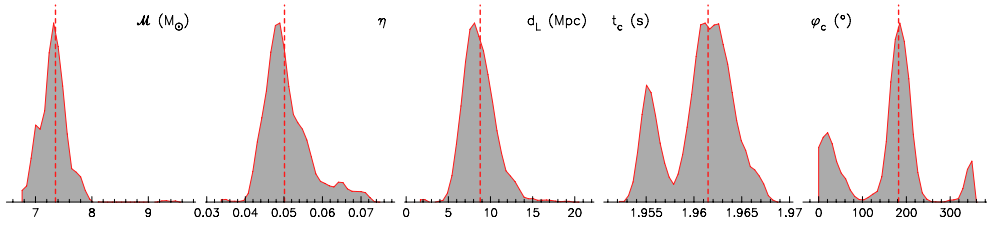
Figure 1. One-dimensional marginalized PDFs for all 15 parameters from our analysis of data sets DS1 (hatched upward; red online) and DS2 (hatched downward; blue online). The vertical dashed lines mark the injection values.

for a GW signal in the data. The difference in the Bayes factor between DS1 and DS2 is attributed to an inherent spread due to different noise realizations, and the uncertainties of our method to estimate the Bayes factor (section 3). The results in this section show an illustrative example, but cannot be used to draw firm conclusions. However, it is clear that they warrant a larger, systematic study of these phenomena with the methods described here.

4.4. Analysis of data sets DS2 and DS3

On 2 November 2006, seismic activity at Hanford and Livingston resulted in a coincident 'glitch' in the data from the H1 and L1 LIGO detectors. These glitches were recovered by the Compact Binary Coalescence detection pipeline at an SNR of 11.3, using non-spinning, stationary-phase-approximation templates, Newtonian in amplitude and 2.0 pN in phase (Abbott *et al* 2009b). We defined the corresponding data set as DS3 in section 4.1 and analysed the data as if they had yielded a GW trigger. The convergence test from section 4.2 yields a 20% convergence rate, which results in our rejection of the results as *not converged*. However, when we nevertheless construct the marginalized one-dimensional PDFs from the

Figure 2. One-dimensional marginalized PDFs of a few selected parameters from our analysis of data set DS3. The vertical dashed lines indicate the median of each PDF.

Table 1. Median and width of the 95%-probability ranges for each parameter of the analyses of data sets DS1 and DS2. The column *recovered* indicates whether or not the 95% range includes the injection value.

		DS1 (synthetic noise)			DS2 (detector noise)		
	Injection	Median	95% width	Recovered	Median	95% width	Recovered
$\mathcal{M}$ ($M_\odot$)	2.99	3.006	0.294	Yes	3.041	0.122	Yes
η	0.107	0.133	0.145	Yes	0.183	0.144	Yes
d_L (Mpc)	28.615	21.240	20.764	Yes	24.144	17.238	Yes
t_c (s)	0.000	−0.013	0.024	Yes	0.006	0.019	Yes
ϕ_c (°)	85.944	189.745	342.398	Yes	185.482	343.175	Yes
α (h)	17.380	11.684	5.349	No	17.786	6.320	Yes
δ (°)	61.642	49.326	64.346	Yes	58.390	39.796	Yes
i (°)	52.753	67.056	110.735	Yes	46.850	122.787	Yes
ψ (°)	11.459	93.162	176.358	Yes	88.706	173.869	Yes
a_{spin1}	0.600	0.658	0.594	Yes	0.804	0.478	Yes
θ_{spin1} (°)	78.463	85.490	83.110	Yes	89.225	85.787	Yes
ϕ_{spin1} (°)	63.025	57.171	335.592	Yes	263.014	345.700	Yes
a_{spin2}	0.400	0.532	0.945	Yes	0.475	0.940	Yes
θ_{spin2} (°)	120.000	94.687	150.544	Yes	89.406	146.101	Yes
ϕ_{spin2} (°)	315.127	181.959	327.603	Yes	184.681	339.071	Yes
M_1 ($M_\odot$)	10.002	8.533	8.849	Yes	6.421	6.536	Yes
M_2 ($M_\odot$)	1.400	1.598	1.277	Yes	2.036	1.564	Yes

data of the two converged chains (because of the small number of data points, the resulting PDFs may not be very accurate), they are similar in appearance to those from DS2 (see figure 2). The Bayes factors in table 2 even suggest that the data set DS3 is more consistent in containing a GW signal than DS2 (with the caveat that the SNRs of DS2 and DS3 were not computed the same way). On the other hand, the low value for the median of η (0.05) corresponds to a mass ratio of 18, which is near the limit of the regime where post-Newtonian expansions are valid. In particular, a small value for eta suggests a slow frequency evolution which may indicate a spike in the frequency spectrum that dominates the signal. In addition, we find that the sky map for DS3 does not display the (parts of a) sky ring that is expected for an analysis using two non-co-located detectors (see e.g. Raymond *et al* (2009)). These results indicate that we should thoroughly verify our tests, such as the convergence criterion described here, using a large number of different glitches.

Table 2. Bayes factors $B_{1,2}$ between the models M_1: a 3.5-pN inspiral waveform embedded in Gaussian noise and M_2: Gaussian noise only (section 4.3) for data sets DS1 and DS2 (see section 4.1).

	DS1 (Gaussian noise)	DS2 (detector data)	DS3 (glitch)
$\log_e B_{1,2}$	52.9	43.5	68.5

5. Conclusions

We have developed the code SPINSPIRAL which can do a complete parameter analysis of the gravitational-wave signals from quasi-circular compact-binary inspirals. We presented an example of the analysis of software injections into both simulated Gaussian noise (DS1) and LIGO-detector data (DS2). We also presented an analysis of a data set containing no injection, but a 'glitch' coincident in two LIGO interferometers (DS3). These examples demonstrate a remarkable similarity between the results obtained from a GW signal injected in Gaussian noise and a similar signal in detector data. The Bayes factors are also similar, where we note that our present technique for computing the Bayes factor yields estimates with significant variance, and more precise estimates should be possible in the future. In addition, we find that although the Markov chains in the analysis of a coincident glitch in LIGO data do not converge, the resulting PDFs could look remarkably consistent with a simulated GW signal. We plan to run our code on a very large number of coincident triggers from the LIGO Compact Binary Coalescence search pipeline (noise events that are somehow being registered as resembling a binary inspiral) in order to get a good sense of how to distinguish them from actual inspirals. We conclude that further, detailed investigations are necessary to ensure that we can rely on the robustness of our tests.

Acknowledgments

References

Abadie J *et al* 2010 arXiv:1003.2480
Abbott B *et al* 2009a *New J. Phys.* **11** 073032
Abbott B P *et al* 2009b *Phys. Rev.* D **79** 122001
Acernese F *et al* 2008 *Class. Quantum Grav.* **25** 184001
Apostolatos T A, Cutler C, Sussman G J and Thorne K S 1994 *Phys. Rev.* D **49** 6274–97
Atchadé Y F and Rosenthal J S 2005 *Bernoulli* **11** 815–28
Buonanno A, Chen Y and Vallisneri M 2003 *Phys. Rev.* D **67** 104025
Cutler C and Flanagan É E 1994 *Phys. Rev.* D **49** 2658–97
Cutler C and Thorne K S 2002 *Proceedings of GR16* (Singapore: World Scientific)
Earl D J and Deem M W 2005 arXiv:physics/0508111
Figueiredo M A T and Jain A K 2002 *IEEE Trans. Pattern Anal. Mach. Intell.* **24** 381–96
Gelman A, Carlin J B, Stern H and Rubin D B 1997 *Bayesian Data Analysis* (Boca Raton, FL: Chapman and Hall)

Gilks W R, Richardson S and Spiegelhalter D J 1996 *Markov Chain Monte Carlo in Practice* (London: Chapman and Hall/CRC)

Hansmann U 1997 *Chem. Phys. Lett.* **281** 140–50

Hukushima K and Nemoto K 1996 *J. Phys. Soc. Japan* **65** 1604

Jaranowski P and Krolak A 1994 *Phys. Rev. D* **49** 1723–39

LIGO Scientific Collaboration 2007 The LSC Algorithm Library https://www.lsc-group.phys.uwm.edu/daswg/projects/lal.html

Newton M A and Raftery A E 1994 *J. R. Stat. Soc.* B **56** 3–48 (http://www.jstor.org/stable/2346025)

O'Shaughnessy R, Kim C, Kalogera V and Belczynski K 2008 *Astrophys. J.* **672** 479–88

Poisson E and Will C M 1995 *Phys. Rev. D* **52** 848–55

Raymond V, Van der Sluys M V, Mandel I, Kalogera V, Röver C and Christensen N 2009 *Class. Quantum Grav.* **26** 114007

Röver C 2007 Bayesian inference on astrophysical binary inspirals based on gravitational-wave measurements *PhD Thesis* The University of Auckland http://hdl.handle.net/2292/2356

Röver C, Meyer R and Christensen N 2006 *Class. Quantum Grav.* **23** 4895–906

Röver C, Meyer R and Christensen N 2007 *Phys. Rev. D* **75** 062004

Skilling J 2006 *Bayesian Anal.* **1** 833–59

Van den Broeck C and Sengupta A S 2007 *Class. Quantum Grav.* **24** 1089–113

Van der Sluys M V *et al* (in preparation)

Van der Sluys M, Raymond V, Mandel I, Röver C, Christensen N, Kalogera V, Meyer R and Vecchio A 2008a *Class. Quantum Grav.* **25** 184011

Van der Sluys M V, Röver C, Stroeer A, Raymond V, Mandel I, Christensen N, Kalogera V, Meyer R and Vecchio A 2008b *Astrophys. J.* **688** L61–4

Van Haasteren R 2009 arXiv:0911.2150

Veitch J and Vecchio A 2008a *Class. Quantum Grav.* **25** 184010

Veitch J and Vecchio A 2008b *Phys. Rev. D* **78** 022001

Veitch J and Vecchio A 2009 arXiv:0911.3820

Willke B and Aufmuth P *et al* 2004 *Class. Quantum Grav.* **21** 417